Fast wavefield extrapolation by phase-shift in the nonuniform Gabor domain

Jeff P. Grossman* and Gary F. Margrave
Geology & Geophysics, University of Calgary
2431 22A Street NW, Calgary, AB, T2M 3X8
grossman@geo.ucalgary.ca

and

Michael P. Lamoureux
Mathematics & Statistics, University of Calgary

ABSTRACT

Wavefield extrapolation for a laterally varying velocity model can be achieved by applying a nonstationary phase-shift filter to an adaptive, nonuniform Gabor transform over the lateral coordinate. A family of adaptive Gabor frames can be constructed from a molecular decomposition of unity, each molecule of the latter being built by conjoining neighbouring atoms from a uniform partition of unity - consisting of translates of a single atom along the lateral coordinate - according to a local stationarity criterion derived from the velocity model.

The resulting extrapolation algorithm - called AGPS (adaptive Gabor phase-shift) - has a computational cost that is proportional to the complexity of the velocity model, while its accuracy is comparable to both NSPS (nonstationary phase-shift) and generalized PSPI (phase-shift plus interpolation). AGPS includes NSPS and PSPI as complementary limiting cases, yet the cost of AGPS ranges from an order of magnitude less to about the same order.

The NSPS and PSPI filters differ to the extent that the functional dependence of the velocity is either on the input coordinates (NSPS) or the output coordinates (PSPI) – in fact, they are spatial transposes of each other. This is why both methods are approximate: indeed, any accurate phase-shift operator in a v(x) medium must allow for velocity variations along the trajectory of a ray. AGPS attempts to address this problem by representing the input and output wavefields as superpositions of windowed components, each of which is approximately stationary with respect to the velocity.

Introduction

This paper has a predominantly qualitative scope. Consequently, an investigation into the underlying mathematical and theoretical background for the new AGPS algorithm has been reserved for a companion paper (Grossman et al., 2002). For a derivation of the new and exact wavefield extrapolator – used here to forward model the propagation of an impulsive wavefield – see Margrave, et al., (2002). Apart from its remarkable accuracy, a distinguishing feature of Margrave's extrapolator is its transitivity through any v(x) medium. By transitivity, we mean that a single depth step yields the same result as the iteration of any number of

intermediate steps does. We use this algorithm as a benchmark to test the performance of three approximate wavefield extrapolation methods: the NSPS and generalized PSPI methods of Margrave and Ferguson, (1999) and AGPS.

The AGPS algorithm includes NSPS and PSPI as complementary limiting cases. Each of these methods applies a velocity-dependent, nonstationary phase-shift filter over each temporal frequency slice of the input data. The two latter filters differ to the extent that the functional dependence of the velocity is either on the input coordinates (NSPS) or the output coordinates (PSPI) – in fact, they are spatial transposes of each other. This is the key reason why both methods are approximate: indeed, any accurate phase-shift operator in a $v(x)$ medium has to account for the fact that the velocity can vary along the trajectory of a ray. AGPS attempts to address this problem by representing the input and the output wavefields as a superposition of windowed components, each of which is approximately stationary with respect to the velocity.

We begin with an overview of the AGPS algorithm, and refer the reader to Grossman, et al. (this volume) for the mathematical details. We then provide a performance analysis for the AGPS, PSPI, and NSPS extrapolators, based on forward-modelled data generated by Margrave's exact extrapolator.

Overview of the AGPS method

AGPS propagates a wavefield from a depth level z to a depth level $z + \Delta z$ by applying nonstationary phase-shift filters to an adaptive spatial Gabor transform of the input data. Given a velocity model, $v(x),$ the first step is to choose a suitable window, or atom. The choice of atom is in itself a current topic of research, (e.g., Feichtinger and Strohmer, 1998, or Grochenig, 2001) but we recommend using a Gaussian or Gaussian-like window, with a halfwidth that is at least large enough to ensure that its sampled version faithfully represents it. This atom is then translated along the discrete *x*-coordinate, one atom centered at each sample point. The resulting suite of windows is rescaled, if necessary, to ensure that its superposition equals one: thus, the translated atoms form a maximal, uniform partition of unity (POU).

Next, this maximal POU is adapted to yield a nonuniform partition of unity, in such a way that the essential nonstationarity of the velocity function is respected. This procedure involves the formation of molecules, or macro-windows, by summing neighbouring atoms over regions that meet a local stationarity measure. The stationarity measure in the current context is simply an acceptable threshold against which the deviation of the velocity from its mean over the current molecule is compared. Thus, if this deviation is less than the threshold, the current atom is conjoined to the current molecule. Each molecule gathers atoms until it encounters a large enough velocity anomaly. The result is an adaptive partition of unity, or molecular decomposition.

In our numerical implementation of the AGPS algorithm, the molecules are defined as follows. Let $\lambda \geq 0$ be a constant, called a threshold, and let the current state of the nth molecule be denoted by M_n^N, where N is the current number of atoms it contains. If x_{n_1} denotes the centre coordinate of the first atom in M_n^N, we may write

$$M_n^N(x) = \sum_{j=n_1}^{n_N} g(x - x_j), \qquad (1)$$

where $n_N = N + n_1 - 1$. Next, define the mean of the velocity over the current molecule by

$$v_{M_n^N} = \frac{\sum_{j=n_1}^{n_N} v(x_j) M_n^N(x_j)}{\sum_{j=n_1}^{n_N} M_n^n(x_j)}. \qquad (2)$$

The stationarity condition with respect to the given threshold λ goes as follows:

$$\text{if} \quad \left| v(x_{n_N+1}) - v_{M_n^N} \right| < \lambda, \quad \text{then}$$

$$M_n^N \rightarrow M_n^{N+1} = M_n^N + g_{n_N+1}; \quad \text{otherwise}$$

$$M_n^N \rightarrow M_n^N \quad \text{and} \quad M_{n+1}^1 = g_{n_N+1}. \qquad (3)$$

Such a molecular decomposition is shown in Figure 1. The illustrated velocity model is representative of all types of variations, ranging from a simple constant to an everywhere discontinuous random function. Note how the atoms cluster near the larger local variations in the velocity. Everywhere else, the atoms 'bond' to form molecules; and their size varies inversely with the magnitude of the local variation of v. Note also that the molecules sum to unity, as desired.

The next step is to use this molecular decomposition to construct a one-parameter family of analysis and synthesis frames for the Gabor transform, indexed by $p \in [0,1]$. For each fixed p, the analysis windows are defined by raising each molecule to the power p. The corresponding dual frame, consisting of synthesis windows, is defined by raising each molecule in the decomposition to the complementary power, $1 - p$.

For example, if the fundamental atom is supported on a finite interval, and $p = 1$, then the molecular decomposition itself forms the analysis frame, and the synthesis windows are boxcars. For $p = 0$, these roles are reversed. However, if the atom is supported on the whole of **R**, (e.g., a Gaussian) then no synthesis (analysis) windows are used if $p = 1$ ($p = 0$). In either case, the analysis and synthesis frames are identical for $p = 1/2$.

The analysis and synthesis frames, constructed in this way, ensure an overall energy and amplitude preserving transformation to the Gabor domain and back(see Grossman et al., 2002). Moreover, with respect to the choice of atom and stationarity measure, the redundancy of the Gabor transform is minimized; hence so is its computation time.
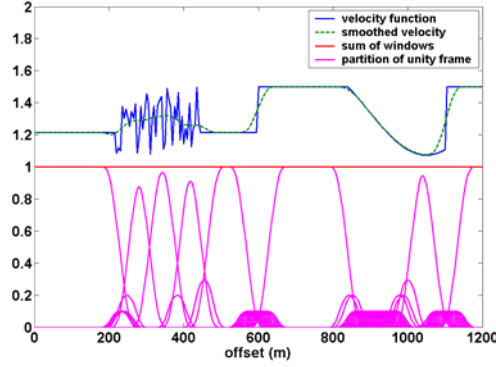
Fig. 1. A demonstration of how the Gabor algorithm achieves an adaptive partition of unity frame (magenta) from a maximal partition of unity, (not shown) which reflects the local nonstationarity of a velocity model. The piecewise-defined velocity model (blue) is representative of all types of velocity variation: constant, random, a jump discontinuity between two constants, and a jump from smooth to constant. The smoothed velocity (dashed green), obtained by convolving the velocity model with a fundamental atom, (any of the smallest magenta windows) acts as a visual aid in comparing the molecules (magenta) to the local velocity variations.

Each frequency slice of the input data, $\psi(x,\omega,z=z_0)$ is then Gabor transformed, $(x \rightarrow (\tilde{x},k_x))$, phase-shifted by $e^{i\Delta z \phi}$, where

$$\phi(\tilde{x},k_x,\omega) = \sqrt{\frac{\omega^2}{[\overline{v}(\tilde{x})]^2} - k_x^2} \, , \tag{4}$$

then inverse Gabor transformed. The result is an estimate of the wavefield, $\psi(x,\omega,z=z_0+\Delta z)$, at depth $z_0+\Delta z$ and frequency ω. After repeating this process for each ω, an inverse Fourier transform over ω gives the desired estimate in space-time coordinates.

The velocity function $\overline{v}(\tilde{x})$ in the dispersion relation (4) is defined, for each $\tilde{x}$, as the mean of the velocity over the molecule centered at $\tilde{x}$. It thus assigns a constant velocity to each molecule in the Gabor decomposition. A key feature that controls the accuracy of the algorithm is the choice of stationarity measure: a large threshold can lead to large molecules; hence, a more coarsely sampled velocity. On the other hand, too strict a measure could lead to higher cost than necessary for the desired accuracy.

Roughly speaking, the balance between the dependence on the input and the output coordinates can be shifted by adjusting the parameter p in [0,1]. However, the situation is more complicated than this, and has yet to be fully understood. In the limit as the window size shrinks to zero, the cases $p=1$ and $p=0$ reduce to NSPS and PSPI, respectively. It turns out that for the examples below, which use compactly supported windows, the best choice is $p=1$. Intuitively, we might expect $p=1/2$ to be optimal, since this implies a symmetric dependence on the input and output coordinates. Experiment suggests that the optimal value of p depends on the choice of window, but this remains an open question.

Examples

Margrave's exact one-way extrapolation algorithm was used as a forward model to upward propagate an impulsive wavefield through a laterally varying velocity field. This impulse response was then inverted, by reverse-extrapolation, using the Exact, NSPS, PSPI, and AGPS extrapolators. The relative costs for two extreme cases appear in *Table 1*. The first is a step between two constant velocities, (*Fig. 2(a)*) and the second involves a velocity function that varies randomly at each offset (*Fig. 2(b)*). In the first case, AGPS outperforms NSPS and PSPI by a factor of six, while all three have similar costs in the second case. The extra cost for the exact algorithm in the random case is small, so its use in complex media may be justified.

Table 1. Comparison of computation times for various extrapolation algorithms. In contrast to the first three methods, the cost of AGPS is proportional to the complexity of the velocity model. The cost of AGPS spans an order of magnitude between the two extremes, namely, the velocity models depicted in Figures 2 and 3.

Extrapolation algorithm	Absolute cost for step/random	Relative cost for step/random
Exact	47.067/46.317	100/100
NSPS - 1 step	3.946/3.675	8.2/7.9
NSPS - 5 steps	20.580/17.545	42.5/37.9
PSPI - 1 step	3.995/3.746	8.2/8.1
PSPI - 5 steps	20.365/19.217	41.9/41.5
AGPS - 1 step	0.601/3.916	1.2/8.5
AGPS - 5 steps	3.245/19.438	6.4/42.0

Fig. 2 shows the velocity models used in our examples, and the corresponding molecular decompositions of unity. Both decompositions are used as analysis frames (so $p=1$) for the nonuniform Gabor transform. The fundamental atoms (black) are Lamoureux windows of order two, (twice differentiable polynomial splines) sampled at 7 points, and the spacing between atoms is 10m.
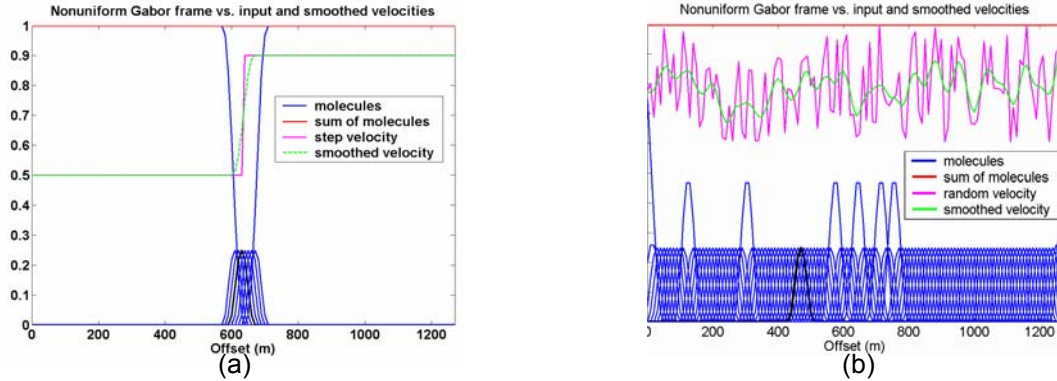
Fig. 2. (a) Molecular decomposition (blue) for a step velocity (magenta), constructed from the fundamental Gabor atom shown in black. The velocity jumps from 2250 m/s to 3750 m/s. (b) Molecular decomposition (blue) for a random velocity (magenta), built from the Gabor atom shown in black. The velocity fluctuates randomly between 1500 m/s and 2500 m/s.

The input wavefield for both examples, shown in *Fig. 3(a)*, consists of eight bandlimited impulses. *Figs 3(b)* and *3(c)* show the exact upward extrapolations of the input wavefield by 200m, using the velocity models of *Figs 2(a)* and *2(b)*, respectively. *Fig.4* shows the results of reverse extrapolating the last two fields with the exact operator. These last two results will serve as benchmarks for comparing the quality of the remaining methods. Aside from some minor numerical artefacts, these images are the best one can hope to obtain (see Margrave et al., 2002).
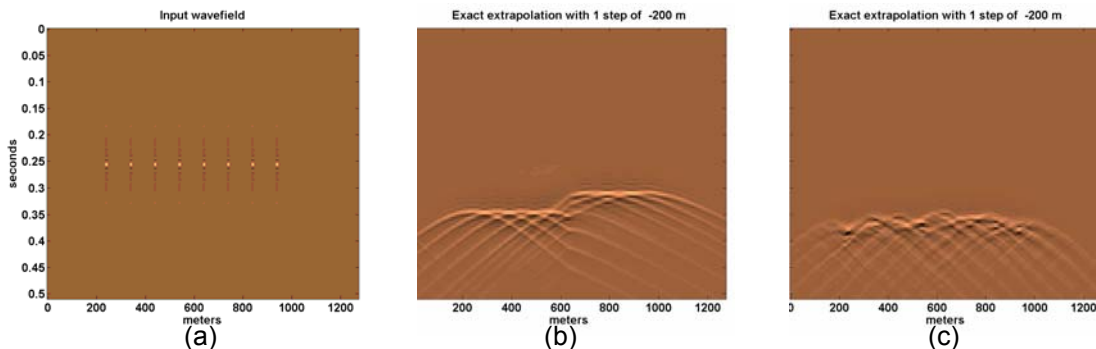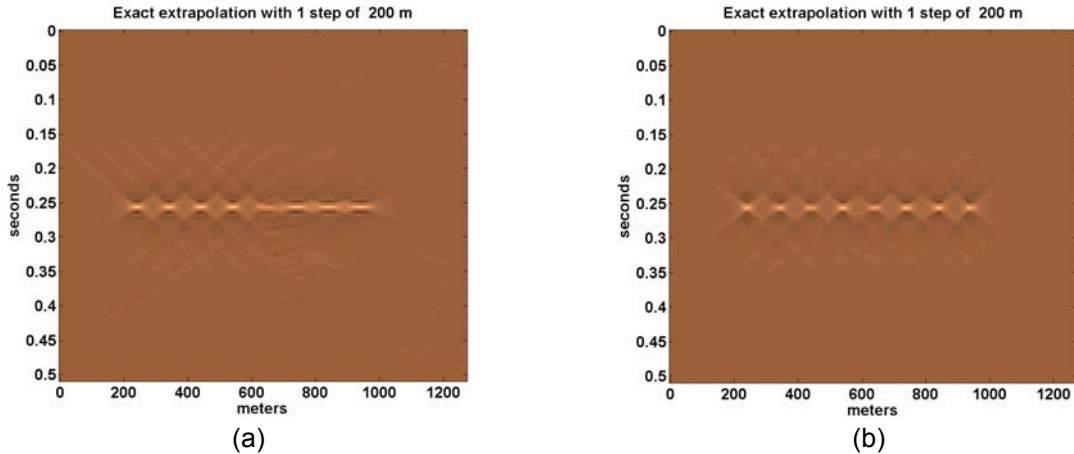

Fig. 3. (a) Input wavefield for two upward extrapolations by 200m, using the exact extrapolator; (b) and (c) show the resulting wavefields, using the velocity models of Figs 2(a) and (b), respectively.

Fig. 4. Inversion of the two wavefields of Figures 3(a) and 3(b): (a) using the velocity model of Figure 2(a), and (b) using the velocity model of Figure 2(b).

Fig. 5 displays the various results of inverse extrapolating the wavefield of Fig. 3(b) - using the step velocity model of Fig. 2(a) - which should be compared to Fig. 4(a). The corresponding computation times are listed in Table 1. The rows contain pairs of results for PSPI, NSPS, and AGPS, respectively; the first column is for a single depth step of 200m, and the second is for five steps of 40m. The last row also shows the corresponding molecular decomposition for the AGPS case.

PSPI gives a reasonable result in both cases, but it introduces an artificial discontinuity in the wavefield at the interface between the two constant velocity blocks. It is well known that PSPI produces this artefact for large depth steps. The results for NSPS are better, particularly since the fifth impulse is more focused. AGPS yields essentially the same result as NSPS, but shows marginally fewer artefacts in the case of five steps. This makes NSPS a bargain – at least for simple velocity models.

Fig. 6 displays the results, in exactly the same format as for Fig. 5, using the input wavefield of Fig. 3(c) and random velocity model of Fig. 2(b). These should be compared to Fig. 4(b). The corresponding computation times are listed in Table 1.

The PSPI and NSPS results 6(a) and (c) are remarkably different. PSPI again introduces discontinuities in the wavefield at every discontinuity in the velocity – hence the randomly scattered appearance of the extrapolation. The result (c) for NSPS shows "migration smiles" that arise due to the use of incorrect velocities. Increasing the number of steps, as in (b) and (d), helps to cure both of these issues. Again, AGPS yields very similar results as NSPS in both cases, although AGPS is slightly better focused, and contains fewer artefacts. Since they use approximate velocities, all three methods tend to misplace the wavefield in time. This effect is most easily observed near discontinuities in the velocity function.

Summary

We showed that AGPS propagates a wavefield from a depth level z to a depth level $z + \Delta z$ by applying nonstationary phase-shift filters to an adaptive spatial Gabor transform of the input data. A family of adaptive Gabor frames was constructed from a molecular decomposition of unity. Each molecule of the latter was built by conjoining neighbouring atoms from a uniform partition of unity - consisting of translates of a single atom along the lateral coordinate - according to a stationarity criterion derived from the velocity model. Each molecule in the resulting Gabor frame was assigned a mean velocity, and then the phase-shift operator was applied, using these velocities, in the nonuniform Gabor domain. This process was repeated for each temporal frequency slice, and the desired extrapolation was represented in the space-time domain by applying an inverse Gabor transform, followed by an inverse Fourier transform over frequency.

The cost of AGPS is proportional to both the complexity of the velocity model and the desired degree of accuracy. Its accuracy is comparable to that of NSPS and PSPI, but its cost is much lower, especially for simple velocity models. For random media, the cost of Margrave's exact algorithm is only marginally greater than the latter three, so its superior quality warrants its use.

Future work

Each of the approximate wavefield extrapolators suffers from a misplacement of the wavefield in time, hence also in depth, especially near vertical discontinuities in the velocity field. However, this can likely be healed somewhat by using a processing technique similar to that used by Stoffa et al., (1990). We first rewrite the phase-shift, $\phi \Delta z$ (see expression (1)) as the sum of a focusing term, $\varphi_f \Delta z$, and a shifting term, $\varphi_s \Delta z$, where

$$\varphi_f = \frac{\omega}{v(x)}\left(\sqrt{1 - \frac{k_x^2}{\omega^2}} - 1 \right) \quad \text{and} \quad \varphi_s = \frac{\omega}{v(x)}. \tag{5}$$

The shifting term is independent of k_x, so it does not vary with propagation direction. Physically, it is responsible for a vertical depth shift of the data, while the focusing term serves as an angle-dependent correction. The idea is to precondition the data by applying the phase-shift operator

$$e^{i\varphi_s \Delta z} \tag{6}$$

in the (x, ω) domain, before implementing the focusing phase-shift filter in the Gabor domain. The second step amounts to replacing expression (1) with

$$e^{i\varphi_f \Delta z} \tag{7}$$

in the AGPS algorithm.

Acknowledgements

References

Bale, R. A., Grossman, J. P., Margrave, G. F., and Lamoureux, M. P., 2002, Multidimensional partitions of unity and Gaussian terrain: CREWES Research Report, *14*.

Feichtinger, H. G. and Strohmer, T., 1998, Gabor analysis and algorithms, theory and applications: Birkhauser.

Gabor, D., 1946, Theory of communication: J. IEEE (London), 93, 429-457.

Gazdag, J., 1978, Wave equation migration with the phase-shift method: Geophysics, Soc. of Expl. Geophys., *43***,** 1342-1351.

Gazdag, J., and Sguazerro, P., 1984, Migration of seismic data by phase shift plus interpolation: Geophysics, *49*, 124 - 131.

Grossman, J. P., Margrave, G. F., and Lamoureux, M. P., 2002, Constructing adaptive nonuniform Gabor frames from partitions of unity: CREWES Research Report, *14.*

Margrave, G. F. and Ferguson, R.J., 1998, Nonstationary filters, pseudodifferential operators, and their inverses: CREWES Research Report, *10*.

Margrave, G. F. and Ferguson, R.J., 1999, Wavefield extrapolation by nonstationary phase shift: Geophysics, *64*, 1067-1078.

Margrave, G. F., Lamoureux, M. P., Gibson, P., Bale, R. A., and Grossman, J. P., 2002, Exact wavefield extrapolation in 2D for $v(x)$: CREWES Research Report, *14*.

Stoffa, P. L., Fokkema, J. T., de Luna Freire, R. M., and Kessinger, W. P., 1990, Split-step Fourier migration: Geophysics, *55*, 410-421.
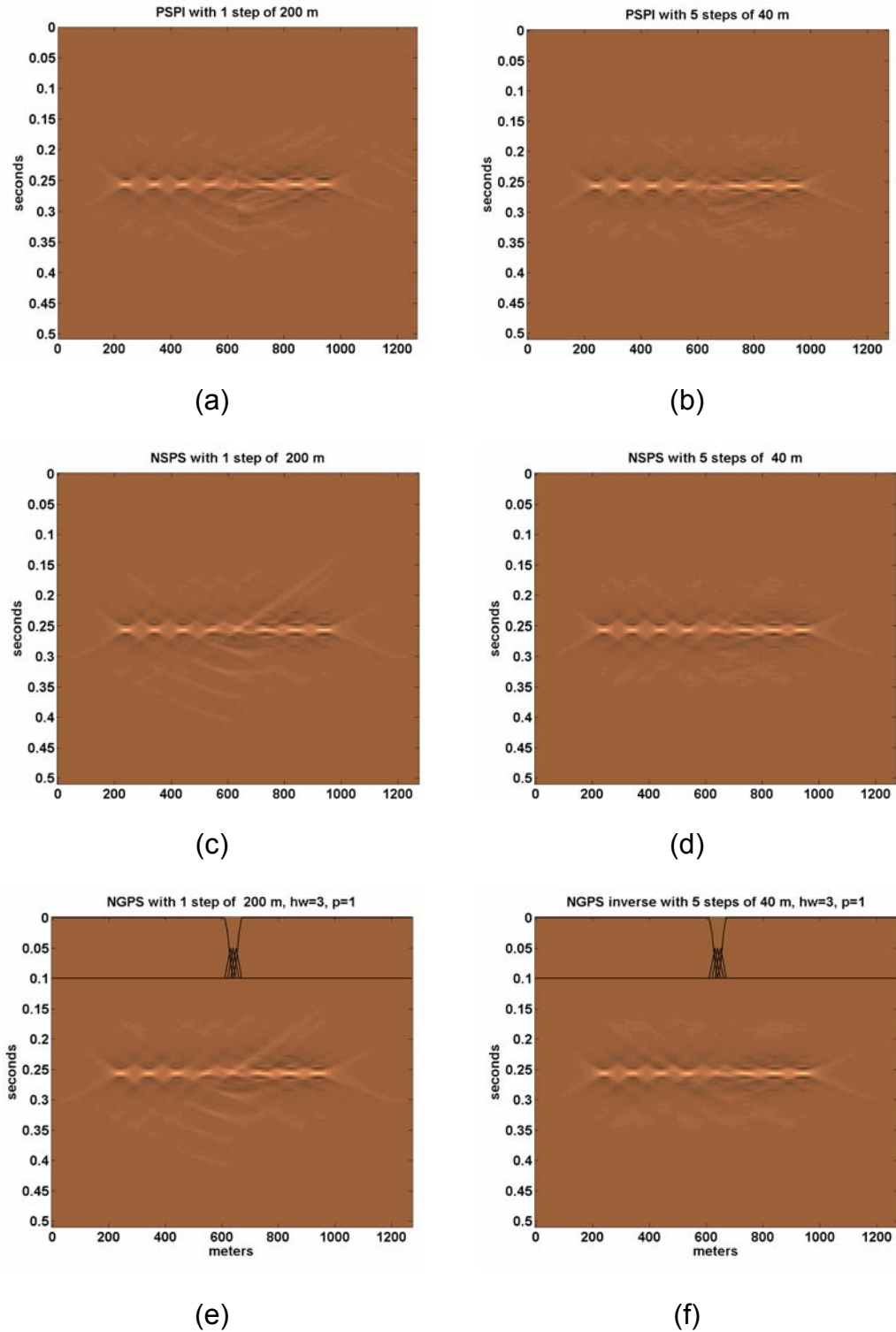
FIG. 5. Results of inverse extrapolating the wavefield of Figure 3(b), using the step velocity model of Figure 2(a). The corresponding computation times are listed in Table 1. The rows contain pairs of results for PSPI, NSPS, and AGPS, respectively; the first column is for a single depth step of 200m, and the second is for five steps of 40m. The last row also shows the corresponding molecular decomposition (black) for the AGPS case. Compare these to Figure 4(a).
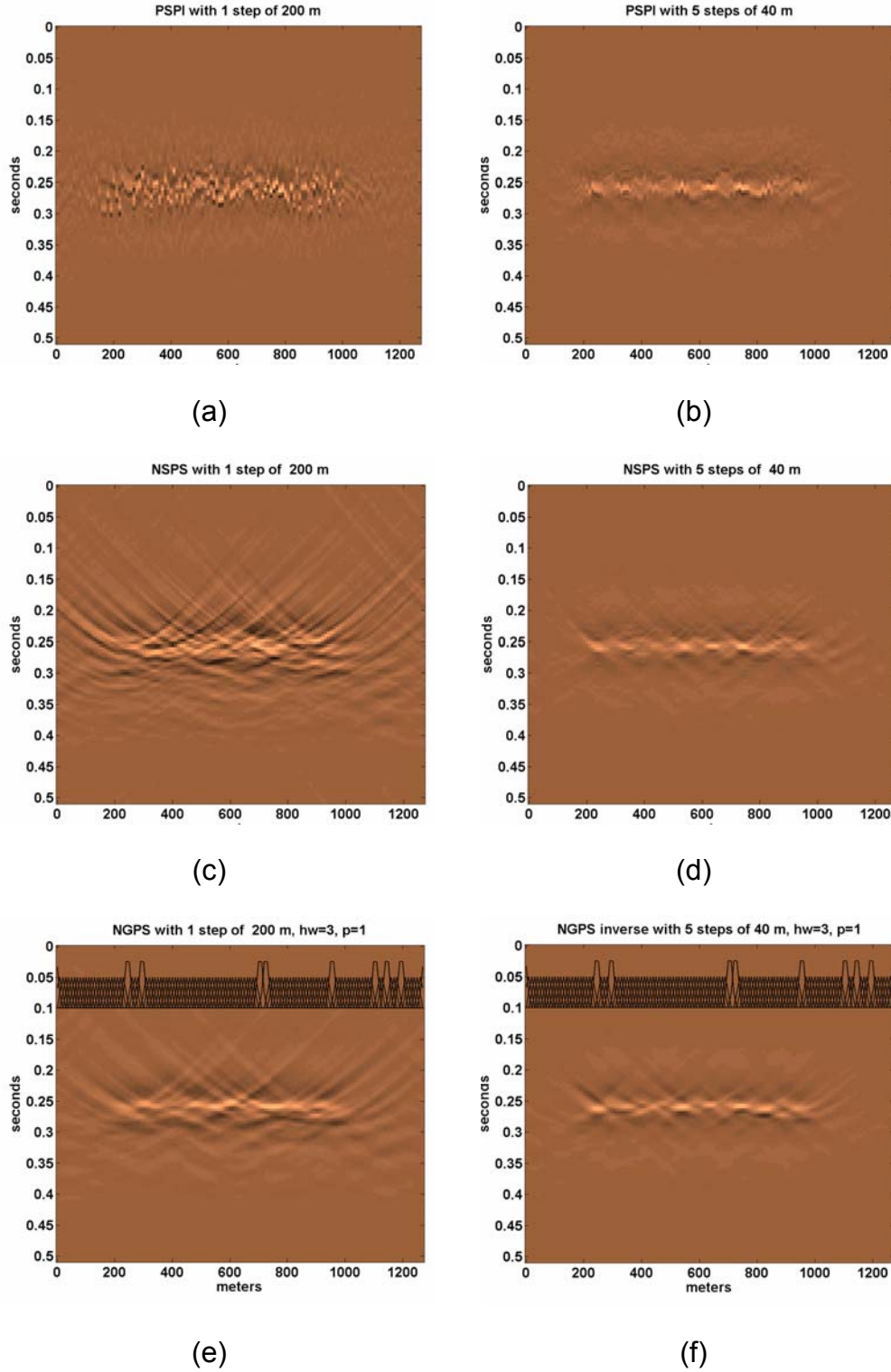
FIG. 6. Results of inverse extrapolating the wavefield of Figure 3(c), using the step velocity model of Figure 2(b). The corresponding computation times are listed in Table 1. The rows contain pairs of results for PSPI, NSPS, and AGPS, respectively; the first column is for a single depth step of 200m, and the second is for five steps of 40m. The last row also shows the corresponding molecular decomposition (black) for the AGPS case. Compare these to Figure 4(b).